Available online at www.sciencedirect.com

ScienceDirect

Ceramics International 40 (2014) 2083–2090

CERAMICS INTERNATIONAL

www.elsevier.com/locate/ceramint

Plasticity and fracture of sapphire at room temperature: Load-controlled microcompression of four different orientations

Alex Montagne[1,2], Siddhartha Pathak[1,3], Xavier Maeder[4], Johann Michler*

EMPA – Swiss Federal Laboratories for Materials Testing and Research, Feuerwerkerstrasse 39, CH-3602 Thun, Switzerland

Received 14 June 2013; received in revised form 15 July 2013; accepted 25 July 2013
Available online 2 August 2013

Abstract

We report the mechanical behavior and deformation mechanisms in sapphire (Al_2O_3) studied using ~1 μm diameter micro-pillar compression experiments performed in situ in a scanning electron microscope (SEM) at room temperature. Four crystallographic orientations: ⟨10 –10⟩, ⟨1 –210⟩, ⟨0001⟩ and ⟨ − 1012⟩ corresponding to *M*, *A*, *C* and *R* planes respectively, were studied. The residual deformations of the four planes were analyzed using Schmid law and geometric observations. Several deformation mechanisms such as cracking and plasticity were observed in our tests, and their probability of occurrence were strongly orientation dependent. Thus, for the same pillar size, pillars oriented along ⟨1 −210⟩ are more prone to deform plastically than those ⟨10 –10⟩ oriented. For pillars exhibiting plasticity, the resolved shear stress achieved just before the load drop was close to one thirtieth of the shear modulus and was consistent with heterogeneous nucleation mechanisms.

Keywords: C. Fracture; C. Mechanical properties; C. Plasticity; D. Al_2O_3; Microcompression

1. Introduction

Sapphire (Al_2O_3) is the second hardest material known (after diamond) and it has many industrial applications such as windows glasses and microelectronics in harsh environment, missiles domes or even transparent armors [1]. Mechanical properties and plasticity of sapphire has been extensively studied since the 70's [2–9] particularly at high temperature [10–18]. Sapphire has a hexagonal compact structure [17,19] where the length a of the basal hexagon is reported to be 4.75 Å and the height *c* of the unit lattice is 12.97 Å, leading to a high aspect ratio (*c*/*a*) equal to 2.73 [20].

Sapphire is known to exhibit 8 slip planes leading to 17 slip systems (see the review in [18]), while other systems with dissociated dislocations have also been reported [10,15–17,21]. The most common reported slipping planes are (with mineralogical symbol): {0001} *C*, {10 –10} *M*, {11 –20} *A*, {01 –12} *R* and {10 − 11} *r* [3,4,6,8,19]. Previous studies have shown the basal or *C* slip to be the dominant slip system for high temperature experiments [10,15,17,18]; however at room temperature *C* slip is difficult to observe [9]. In addition sapphire crystal exhibits a significantly higher strength when deforming parallel to the [0001] direction and is not able to deform plastically. Several authors linked this to crystallographic properties, *i.e.*, when *C* is the compression plane, slip systems in *C*, *A* and *M* planes present a Schmid factor equal to zero, thus a lot of systems are unable to help the deformation [8,22]. Nanoindentation studies have also shown that fracture and twinning are the main mechanisms responsible for deformation at room temperature. Two types of twinning systems are typically reported in sapphire: basal (*C*) and rhombohedral (*R*) twinning [10,16].

*Corresponding author.
E-mail addresses: pathak@lanl.gov, siddharthapathak@gmail.com (S. Pathak), johann.michler@empa.ch (J. Michler).
[1]Both authors equally contributed to this work.
[2]Current address: Laboratoire Interdisciplinaire Carnot de Bourgogne, CNRS – Université de Bourgogne, 9 avenue Alain Savary, 21 000 Dijon, France.
[3]Current address: MPA-CINT Center for Integrated Nanotechnologies, Los Alamos National Laboratory, P.O. Box 1663, MS – K771, Los Alamos, NM, 87545, USA. Tel.: +505 667 2082; fax: +505 665 9030
[4]Current address: CSEM Center Suisse d'Electronique et de Microtechnique SA, Jaquet-Droz 1, 2002 Neuchâtel, Switzerland.

0272-8842/$ - see front matter © 2013 Elsevier Ltd and Techna Group S.r.l. All rights reserved.
http://dx.doi.org/10.1016/j.ceramint.2013.07.121

The deformation mechanisms in sapphire have been traditionally difficult to examine due to its relatively high strength and its brittle nature. The advent of micro-mechanical testing over the last two decades, such as nanoindentation experiments [10,16], have helped to alleviate this problem since a lower load is required to deform the micron-sized volumes in these tests. Micro-pillar compression tests are particularly advantageous in this respect since they can be used to induce a brittle-to-ductile transition in the material response by controlling the volume of the interrogated material [23–31]. More recently, the technique has been applied to gain new insights into the onset of deformation mechanisms in brittle materials using in situ Raman spectroscopy [32,33]. Micro compressions of metals show an increasing yield strength as the pillar size is decreased [25–27]. Several authors have associated the increase in yield strength in these experiments to the lack of dislocation sources (similar to what has been reported for whisker deformation [34–36]) suggesting that the deformation is controlled by dislocation nucleation. Other researchers such as Greer and Nix [28,29] have proposed a model for "dislocation starvation hardening" for gold micropillar compressions. In this model, stress induced by the contact of the flat punch push out preexisting dislocations from the pillar and leaves a dislocation-free crystal able to support higher stresses. Nevertheless, the yield strength never reaches the so called theoretical shear stress set to $G/10$ (with G the shear modulus) but a lower value closer to $G/30$. Bei et al. [37] linked the inability to reach the theoretical shear stress to the use of focused ion beam (FIB) which is the most common technique for pillar fabrication. These authors showed that defects induced by FIB milling in Mo-alloy pillar help to decrease the stress for dislocation nucleation, and this effect is more visible as the pillar size decreases. The nature of these defects could be point defects, amorphization or even dislocations [38–40]. Moreover, previous studies in semi-conductors have reported that nucleation from surface causes a decrease in the critical stress [41]. It is then obvious that in reduced structures, such as micropillars, the surfaces have a predominant influence. Bei et al. [42] applied the work of Beltz et al. [43] to the compression of micropillars and attributed the "low" yield stress (as compared to the theoretical shear stress) to the fraction of the dislocation loop generated. That is, during compression of micro-pillars, dislocations are nucleated from the surface and thus a half or a quarter loop is nucleated instead of a full loop as in other test modes such as nanoindentation. They estimated that the critical shear stress is reduced by a factor of two and three for a half and a quarter dislocation loop, respectively.

As mentioned earlier, micro-pillar compression experiments offer the opportunity to study some interesting size effects, in particular the brittle to ductile transition temperature (BDTT). Recent works in brittle materials such as silicon [44] or gallium arsenide [31] show a lowering of the BDTT when the diameter of the pillar is reduced. For a diameter lower than a critical value, pillars show a ductile behavior with considerable dislocation activity. On the other hand, for pillars with diameters greater than the critical value the deformation is mainly governed by crack nucleation and propagation.

Unlike other micro-mechanical testing geometries (such as nanoindentation), the stress state in micropillar compressions is mostly uniaxial, which allows the determination of the resolved shear stress (RSS) acting on slip planes using the Schmid's factor analysis [45,46]. However as the pillar size decreases so does the probability of the presence of dislocation sources within the pillar volume. Ng and Ngan [47] proposed a numerical model to study the correlation between the operative slip system and the Schmid factor in face centered cubic structures. They showed a competition between the mechanisms of dislocations glide and nucleation, always in favor of the glide. Consequently the active slip system is firstly one with preexisting dislocation and then the one with the highest Schmid factor.

Although the mechanical properties of bulk sapphire have been studied extensively [2–9], its mechanical behavior at the micron and sub-micron length scales have generally been restricted to nanoindentation experiments [10,16]. To our knowledge no observations of compression of micron-sized sapphire pillars at room temperature have been reported. Here we present the results of our investigations on the different deformation modes of four common orientations in sapphire, namely the $\{0001\}$ C, $\{10\,{-}10\}$ M, $\{11\,{-}20\}$ A, and $\{01\,{-}12\}$ R planes, at room temperature using micro-pillar compression experiments. By decreasing the pillar sizes to $\sim$1 μm diameter we are able to study the plastic behavior of this normally brittle material under compression.

2. Experimental procedure

2.1. Sample preparation and compression

Sapphire single crystals of 4 different orientations, namely the $\{0001\}$ C, $\{10\,{-}10\}$ M, $\{11\,{-}20\}$ A, and $\{01\,{-}12\}$ R planes, grown by the Kyropoulos method were investigated. The samples were in the form of discs of 3 cm diameter and 3 mm thickness with both sides polished. At least 5 micro-pillars were fabricated using the focused ion beam technique (FIB SEM Lyra from Tescan, Czech Republic) in each of the 4 samples. For all 4 crystal orientations the fabricated micro-pillars were about 3 μm in height with a diameter of 1 μm, or an aspect ratio of about 1:3. Due to the limitations of the fabrication technique the pillars were not perfect cylinders, i.e. the outer walls were not perfectly parallel to the pillar axis. This taper angle was measured to be around 4°, making the uniaxial stress state in the pillars inhomogeneous.

The sapphire micro-pillars were compressed inside a custom-built indenter [33,48] using a 5 μm diameter flat punch indenter tip. Experiments were been performed in situ under a Zeiss DSM962 scanning electron microscope (SEM) (Oberkochen, Germany). The in-situ technique allows proper alignment of each individual pillar under the flat punch. The compression tests were performed at a 1 nm/s displacement rate, and the force and displacement values were continuously recorded. A typical stress-displacement curve is shown in Fig. 1. The study is focused on the stress analysis of the pillars, thus displacement has not been converted into strain. Furthermore the exact procedure for the conversion of displacement to strain in micro-pillar compressions

is still subject to debate [49]. The tests were continuously monitored inside the SEM and pillar images were taken both before and after compression. The active slip systems were determined using crystallographic and geometric considerations with the help of the Schmid's law. We assumed the origin of dislocations to be at the upper part of the slip step (where the smaller size of the pillar cross-section results in a higher uniaxial stress). We also assume that the justification of the Schmid's law breakdown by Ng and Ngan [47] cannot be considered here due to the very low density of pre-existing dislocations [50].

The crystal orientations were determined using electron back scattered diffraction (EBSD) obtained using a Zeiss DSM 962 scanning electron microscope (SEM). These orientations are represented on the SEM images by a white 2D projection of the hexagonal lattice.

2.2. Stress analysis

Assuming uniaxial compression, the stress acting on a slip system can be resolved using the Schmid factor m [45,46]

$$m = \cos\varphi \cos\lambda \quad (1)$$

Where φ and λ are angles between the loading axis and the slip plane normal, and between the load axis and the slip direction, respectively. Thus, the resolved shear stress τ_{RSS} acting on the entire plane is given by

$$\tau_{RSS} = mp \quad (2)$$

Where p is the uniaxial stress, defined as the ratio between the force and the contact area. The shear modulus was set to 157 GPa [51] for all orientations in order to simplify the analysis.

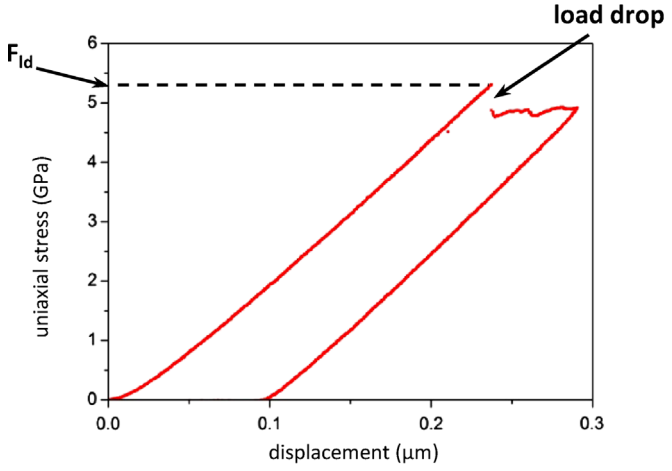

Fig. 1. Typical uniaxial stress – displacement curve on sapphire. The load drop (ld) is indicated by an arrow.

3. Observations and discussions

Micro-pillar compression tests were performed on the *C*, *R*, *A* and *M* orientations of sapphire and a typical stress – displacement curve is shown in Fig. 1. The stress reported here corresponds to the uniaxial stress calculated using the diameter of the pillar-top, since the stresses are highest at this point due to the taper in the pillars. The loading curves typically exhibited a load (stress) drop, marking the transition from reversible to irreversible deformation, usually associated with dislocation activity. When pillars are unloaded before any load-drop, loading and unloading curves are perfectly superimposed and no residual deformation (steps, cracks, etc.) was observed. The load (stress) drop is thus a good benchmark to indicate the start of irreversible deformation. It is marked by an arrow on the stress-displacement curve shown in Fig. 1. The value for the critical stress calculations was taken from the first load drop, corresponding to F_{ld} on Fig. 1.

We observed two different deformation behaviors in the sapphire micro-pillars. In one case SEM images revealed cracks to be present in the deformed pillars, whereas in the second case the pillars presented clear and well defined glide planes as indicated by a distinct line on the pillar surface (for example see Fig. 2). Furthermore in the latter case, the uniaxial stresses at the load drop (F_{ld}) were greater; these values were also highly consistent over multiple tests unlike in the first case where a larger spread was observed. These observations lead us to believe that the deformation behavior is governed by plasticity in the latter case and not by fracture based on a statistical distribution of preexisting flaws (as in the former case). In the following analysis, we concentrate our efforts on the data obtained from pillars exhibiting exclusively the characteristics of the latter group. The results of our analysis are summarized in Table 1.

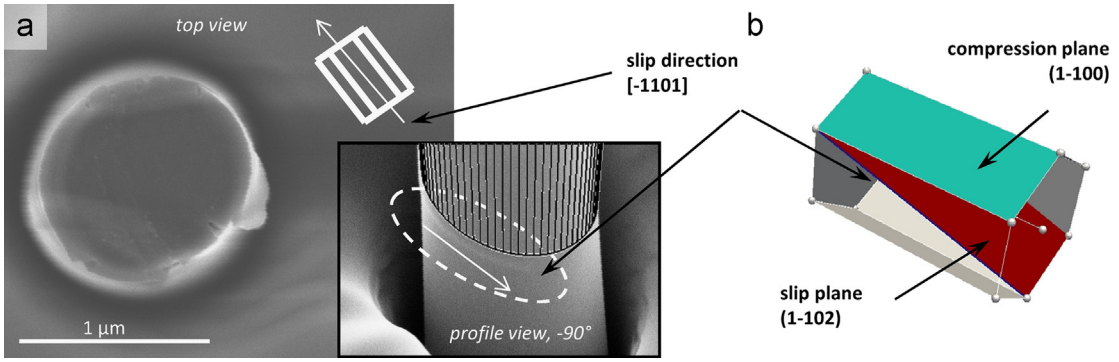

Fig. 2. Pillar after compression on *M* plane, (a) top view SEM image with a symbolized plane view of the hexagonal lattice; a profile view rotated from 90° is given in inset, the slip direction is indicated by continuous white arrows and (b) schematic 3D view of the hexagonal lattice with crystallographic planes and orientations.

Table 1
Uniaxial stress observed at load stress drop for each orientations, with corresponding slip systems and resolved shear stress (RSS), average values of uniaxial stress and RSS are obtained from n experimental values (ductile deformation).

Compression plane	Uniaxial stress (GPa)	Active slip system	RSS (GPa)	n	N
M	13.6	$\{1\ -102\}1/3\langle 1101\rangle$	6.1	2	6
A	11.1	$\{1\ -101\}1/3\langle 01\ -11\rangle$	4.3	3	4
C	23.7	$\{01\ -12\}1/3\langle 0\ -111\rangle$	10.7	4	8
M	13	–	–	3	4

N is the total number of pillar deformed (brittle and ductile deformation). RSS values were calculated from the uniaxial stresses using Eq. (2).

3.1. Compression on M plane

The average uniaxial stress at the load-drop during compression on the M face was measured to be 13.6 GPa (average of 2 tests). Fig. 2 shows the SEM image of a pillar after compression along the [1 −100] direction. Fig. 2a shows the top SEM view of the compressed pillar; the schematic in the upper right corner shows the projected plan view of the hexagonal lattice giving the orientation of the crystal. The profile view in the inset shows the intersection between the pillar's wall and the slip plane (circled). Two planes are closely aligned to this feature: r and R. These two planes lead to five different slip systems. With respect to the Schmid factor analysis, two slip systems exhibited a null value. The slip system $\{1\ -102\}1/3\langle -1101\rangle$ was found to have the highest value, equal to 0.45. Furthermore the observed slip steps are consistent with this system. The other two remaining systems showed values 25% and 55% lower. This indicates that the $\{1\ -102\}1/3\langle -1101\rangle$ is the prominent slip system for this orientation. Note that this slip plane corresponds to the R plane of sapphire and Fig. 2b shows the schematic 3D view of the hexagonal lattice showing slip plane and direction. Slip direction is also pointed out by the white arrow on SEM images. Finally, the resolved shear stress acting in this system (Eq. (2)) was calculated to be about 6.1 GPa.

3.2. Compression on A plane

The average uniaxial stress at the load drop for compression on the A plane was 11.1 GPa. Fig. 3 shows a pillar after compression parallel to the A plane [2 −1 −10]. Slip steps are clearly visible in Fig. 3a (dashed black arrows). We focus our attention on the slip step produced on the top of the pillar. Physically, this line is the intersection between the compression plane A, and the slip plane. For clarity, this line has been highlighted by a white dashed line on Fig. 3a. The angle measured between this slip line and the c axis of the hexagonal lattice is 35°. The only plane that is able to produce this angle when intersecting the A plane, is the r plane (1 –101). The intersection between both A and r planes is the line [01 −11] which made an angle of 33° with the [0001] axis. In the r plane two systems are possible, but in the present configuration only the system $\{1\ –101\}1/3\langle 01\ –11\rangle$, presenting a Schmid factor equal to 0.38, is consistent with experimental observations. We note that another slip system (in the M plane) present a higher Schmid factor of 0.43. But the M plane is unable to produce this kind of slip step with the A plane. In addition the Schmid factor of the active system is only 10% lower than that of the M plane and hence adherence to the Schmid's law can be explained by experimental uncertainties. Finally, the resolved shear stress (calculated using Eq. (2)) acting on $\{1\ –101\}1/3\langle 01\ –11\rangle$ is 4.3 GPa (averaged over 3 values).

3.3. Compression on C plane

Micro-pillar compressions on the C plane led to an averaged uniaxial stress at the load drop of about 23.7 GPa. Fig. 4a shows a pillar compressed on the C orientation. The slip plane {01 –12} was determined using geometric observations. The profile view in Fig. 4b clearly shows a big translation of the top of pillar, resulting in a large step. The white arrows in Fig. 4a and b represent the projection of the slip direction on the C plane. In the {01 –12} slip plane, the only direction which gave a perpendicular projection to a side of the basal hexagon was the ⟨0 –111⟩ direction. Thus the slip system activated here was the $\{01\ –12\}1/3\langle 0\ –111\rangle$as schematically represented in Fig. 4 c. The Schmid's factor for this slip system is 0.45 (from Eq. (1)), it is one of the very few to be non-zero and is the highest value for this orientation. The resolved shear stress acting on this slip system was calculated to be 10.7 GPa (averaged value on 4 tests). Nanoindentation experiments on (0001) Al_2O_3 of Mao et al. [2] showed another preferred operative slip system (same plane but with a different slip directions): $\{01\ –12\}1/3\langle -2021\rangle$. But from the observations made here it is clear that the shear direction reported by Mao et al. [2] is not compatible with the experimental observations of Fig. 4a.

3.4. Compression on R plane

Fig. 5 presents the results of compression tests on the R plane. The uniaxial stress at the load drop is about 13 GPa (average of 3 tests). The residual deformation observed at the bottom of the pillar in Fig. 5a looks different from the other three orientations described above. Instead of a sharp line the pillar exhibits a "stair shaped" surface. Nevertheless the deformation was identified to take place in the A planes. But we found no slip direction consistent with a glide in A plane that can explain the profile of the deformation. In addition these mechanisms mainly took place at the bottom of pillars (2 of them) and could be probably linked to the interaction between the pillar and the substrate below.

In addition, a clear line is observed in the SEM image in Fig. 5b which has the appearance of a slip step. Two points need to be noted here: first, the deformation seems to take place in the same plane as in the pillar bottom; and second, crack formation was observed at the intersection of this slip plane with the top of the pillar. A closer observation of the

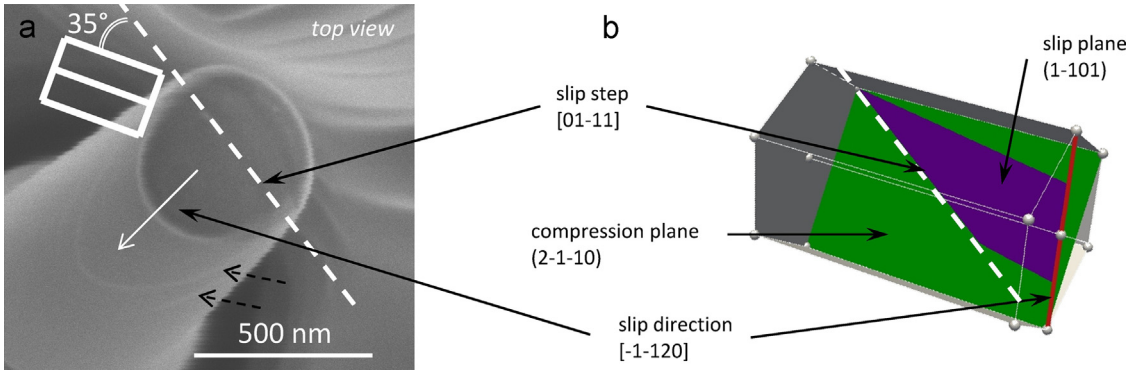

Fig. 3. Pillar after compression on *A* plane, (a) top view SEM image with a symbolized plane view of the hexagonal lattice, the intersection of the slip plane and the surface *A* is marked by the white dashed line, the slip direction is indicated by continuous white arrow and (b) symbolized 3D view of the hexagonal lattice.

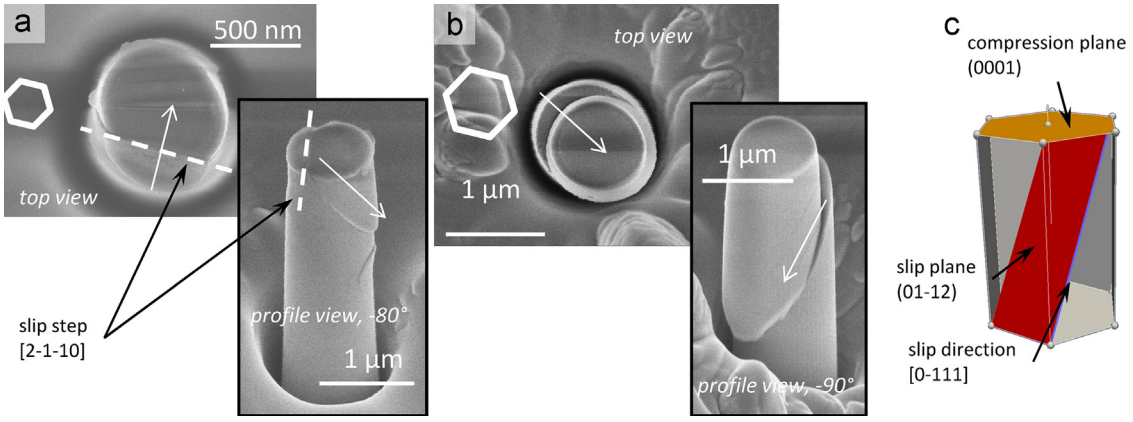

Fig. 4. Two pillars after compression on *C* plane, (a) and (b) top view SEM image with a symbolized plane view of the hexagonal lattice, and profile SEM view, the slip direction is indicated by continuous white arrows. The slip step is clearly visible in (a) whereas the slip direction is more observable in (b) and c) symbolized 3D view of the hexagonal lattice.

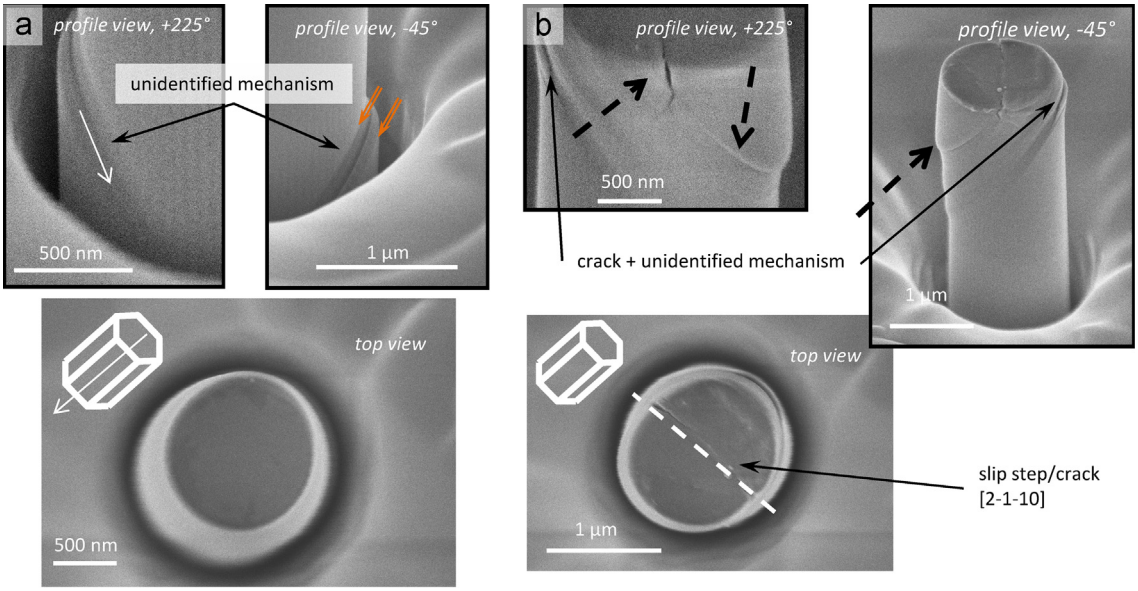

Fig. 5. SEM images of pillars after compression on the *R* plane, (a) top and two profiles views showing an unidentified mechanism of deformation whose width is highlighted by two double orange arrows and (b) top and profiles views showing a second pillar with slip marked by bold dashed arrows, the corresponding slip step is melting with a crack in the [2 −1 −10] direction. (For interpretation of the references to color in this figure legend, the reader is referred to the web version of this article.)

SEM image in Fig. 5b shows the slip step to be continuous on both sides of the crack. This is highlighted by two bold dashed black arrows. This might suggest that in this particular case a crack may have been nucleated after the nucleation and propagation of dislocations. We also note a light "stair shaped" deformation along with crack formation in the upper part of the pillar in Fig. 5b. Everything taken together, this orientation shows multiple deformation mechanisms belonging to different origins, and the sequence of events happening under compression is not clear. Thus it is difficult to conclude in terms of a preferential mechanism for this case.

4. Discussion

This work reports a systematic study of the deformation modes under uniaxial compression on four different crystallographic orientations in sapphire. Sapphire is a ceramic exhibiting a wide variety of deformation mechanisms including cracks, twinning, and dislocations. When macroscopic samples of sapphire are deformed at room temperature, the dominating mechanisms are crack formations and propagation, as is the general characteristics of majority of brittle materials. However, as the temperature of deformation is increased beyond the brittle–ductile transition temperature (BDTT) the brittle material becomes ductile and exhibits plasticity. Other than temperature, several different solutions exist to lower the BDTT, such as applying an external confinement field (gas pressure, etc.) or an internal elastic field (nanoindentation). Recent studies have also shown that reducing the size of the sample can also lower the BDTT, as shown previously for 300 nm diameter pillars of silicon which are able to deform plastically at room temperature [44]. This demonstrates the usefulness of micro-pillars for the study of the plasticity at room temperature without applying pressure to prevent fracture. Moreover micro-pillar testing also allows in-situ observations in the SEM during the experiments thus enabling simultaneous correlations between the evolution of the deformation behavior and their corresponding stress–strain response.

Mechanisms of plasticity at these length scales are still under debate, and researchers have speculated about the competition between dislocation activation and nucleation. Furthermore the role of surface-dominated mechanisms is still not completely understood. The theoretical elastic limit of $G/10$ has been commonly reported as a benchmark for dislocation nucleation. When dislocation activity is reported at a lower stress, dislocation nucleation from a source of dislocation glide is generally invoked.

In this work we analyze the influence of crystal orientation on the deformation mechanisms in sapphire. All orientations exhibit a competition between crack formation vs. dislocation activity. Focusing on tests which present evidence of clear plastic deformation, compressions on *M* and *A* planes show that the resolved shear stress (RSS) reached just before the load drop is around 5 GPa corresponding to a value close to $G/30$. Three possible assumptions can therefore be made. (i) It could be expected that the stress induced by the contact of the flat punch simply moved the preexisting dislocations already present in the pillar. Knowing that a full Burgers vector is approximately 0.5 nm [18] in sapphire and that the residual deformation can reach several nanometers (for example see Fig. 5b), the necessary number of pre-existing dislocations in the same plane is thus very large (from tens to several hundreds) and therefore improbable. (ii) A second hypothesis is the activation of a dislocation source. We consider now the probability of initiating plastic deformation in a pillar; for the *M* orientation 6 pillars were deformed and 2 of them exhibit plasticity, which gives a probability of 0.3. The 4 remaining pillars show cracks prior to measurable plastic deformation. With the same approach probabilities of initiating plastic deformation are 0.8 and 0.5, for the A and C orientations respectively. According to the work of Perner et al. [50], the dislocation density in sapphire grown by the Kyropoulos method is lower than $10^{-4}\,\mathrm{cm}^{-2}$. This range of dislocation density leads to one dislocation every 10.000 pillars. Consequently, there is a great mismatch between the probability of initiating plasticity vs. the availability of possible dislocation sources (i.e. the presence of dislocations plus a configuration in which these dislocations can act as a source). So it can be concluded that pillars are initially dislocation free and have no other way to deform plastically than involving dislocation nucleation. (iii) Accordingly the third hypothesis is that dislocations were nucleated by the stress field of the punch. The low critical stress exhibited by the pillars (which is significantly lower than G/10) could be explained by the (tapered) geometry and the size of objects and/or by topographic irregularities created by the ion beam milling. It is known that during FIB milling pillars are also subjected to ion implantation and defect nucleation [37,38,52]. We used Stopping and Range of Ions in Matter (SRIM, [53]), based on Monte-Carlo simulations, to get an estimate of damages induced by the FIB milling. Parameters used for the simulations were 20 and 50 eV for displacement energy of aluminum and oxygen atoms respectively [54] and a density of $3.98\,\mathrm{g\,cm}^{-3}$ [19]. Crystallography was not taken into account and atoms were randomly distributed. Our results show a 20 nm implanted layer thickness with a high concentration of vacancies surrounding the entire pillar. This suggests that the strong vacancies gradients, implantation and topographic defects may concentrate stress and help in nucleating dislocations, thereby resulting in a lower critical stress. Moreover it has been proposed that, unlike in nanoindentation where full dislocation loops are nucleated which require a higher stress, only partial dislocation loops are nucleated in micro-pillar deformations, and thus a lower stress level may be sufficient [42]. Thus, according to the above arguments, we believe heterogeneous nucleation to be the probable cause for initiation of plasticity in sapphire micro-pillar deformation.

We hypothesize that since all pillars have the same dimensions of 1 μm diameter, but not the same probability to deform plastically, the brittle–ductile transition in sapphire is probably orientation dependent. It can be assumed that reducing the size of the pillar will increase the probability of plastic deformation for all orientations and in particular for compression on the *M* plane.

As expected compression along the ⟨0001⟩ direction exhibits the highest strength [8,22]. Surprisingly, cracks were expected

but under compression some pillars exhibited only plastic deformation without any brittle behavior.

Contrary to Schmid's law, active slip systems were not always those with the highest Schmid factor. Following the results of Ng and Ngan [47], Schmid law is only valuable when all slip systems contain mobile dislocations. As discussed above, in our work plasticity mechanisms are governed by nucleation and not by glide. Thus one might expect the nucleation stresses to be different from one system to the next, leading to the activation of low Schmid factor system with a low critical nucleation stress.

While the work presented here is a first report on the deformation behavior of sapphire under micro-compression, future endeavors will focus more on the study of BDTT in sapphire as a function of temperature (high temperature micro-compression experiments) coupled with systematic TEM observations.

5. Summary and conclusions

We investigated the deformation behavior of micro-pillars of sapphire of 4 different crystallographic orientations. Our results show that compressions in micron-sized pillars of sapphire ($\sim$1 μm diameter) can induce plastic behavior in this brittle material. Especially significant is the plasticity exhibited by the *C* plane in sapphire which is strongest orientation in a hexagonal crystal and has the lowest number of available slip systems. The brittle-to-ductile transition was also found to be orientation dependent; thus for some orientations in sapphire the 1 μm diameter of the pillars remained too large for an exclusive deformation by dislocation activity. Post deformation SEM imaging of the pillars exhibiting plasticity revealed typical deformation by slip. When plastic deformation occurred the slip system was submitted to a stress three times lower than the theoretical shear stress level and is close to *G*/30. Our analysis shows that plasticity in sapphire pillars is probably nucleation dominated (more precisely heterogeneous nucleation), resulting in a relatively lower stress level required for their activation as compared to their theoretical shear strength.

Acknowledgments

This work has been supported by the CTI/KTI Project number 10610.2 of the Swiss Confederation. Authors are grateful to Dr. Christoph Niederberger for the EBSD measurements. SP gratefully acknowledges funding from the Los Alamos National Laboratory Director's Postdoctoral Fellowship during the writing of this manuscript.

References

[1] C.D. Jones, J.B. Rioux, J.W. Locher, H.E. Bates, S.A. Zanella, V. Pluen, M. Mandelartz, Large-area sapphire for transparent armor, American Ceramic Society Bulletin 85 (2006) 24.

[2] W.G. Mao, Y.G. Shen, C. Lu, Deformation behavior and mechanical properties of polycrystalline and single crystal alumina during nanoindentation, Scripta Materialia 65 (2011) 127.

[3] N.I. Tymiak, W.W. Gerberich, Initial stages of contact-induced plasticity in sapphire. I. Surface traces of slip and twinning, Philosophical Magazine 87 (2007) 5143.

[4] N.I. Tymiak, W.W. Gerberich, Initial stages of contact-induced plasticity in sapphire. II. Mechanisms of plasticity initiation, Philosophical Magazine 87 (2007) 5169.

[5] C. Lu, Y.-W. Mai, P.L. Tam, Y.G. Shen, Nanoindentation-induced elastic–plastic transition and size effect in α-Al_2O_3 (0001), Philosophical Magazine Letters 87 (2007) 409.

[6] R. Nowak, T. Sekino, K. Niihara, Surface deformation of sapphire crystal, Philosophical Magazine A 74 (1996) 171.

[7] R. Nowak, M. Sakai, The anisotropy of surface deformation of sapphire: continuous indentation of triangular indenter, Acta Metallurgica et Materialia 42 (1994) 2879.

[8] J.D. Clayton, A continuum description of nonlinear elasticity, slip and twinning, with application to sapphire, Proceedings of the Royal Society A 465 (2009) 307.

[9] Kollenberg, Plastic deformation of Al_2O_3 single crystals by indentation at temperatures up to 750 °C, Journal of Materials Science 23 (1988) 3321.

[10] K.P.D. Lagerlof, A.H. Heuer, J. Castaing, J.P. Riviere, T.E. Mitchell, Slip and twinning in sapphire (alpha-Al_2O_3), Journal of the American Ceramic Society 77 (1994) 385.

[11] B.Y. Farber, S.Y. Yoon, K.P.D. Lagerlöf, A.H. Heuer, Microplasticity during high temperature indentation and the peierls potential in sapphire (α-Al_2O_3) single crystals, Physica Status Solidi A 137 (1993) 485.

[12] M.V. Klassen-Neklyudova, V.G. Govorkov, A.A. Urusovskaya, N.N. Voinova, E.P. Kozlovskaya, Plastic deformation of corundum single crystals, Physica Status Solidi B 39 (1970) 679.

[13] M. Castillo Rodríguez, J. Castaing, A. Muñoz, P. Veyssière, A. Domínguez Rodríguez, α-Al_2O_3 sapphire and rubies deformed by dual basal slip at intermediate temperatures (900–1300 °C) II. Dissociation and stacking faults, Acta Materialia 57 (2009) 2879.

[14] M. Castillo Rodríguez, J. Castaing, A. Muñoz, P. Veyssière, A. Domínguez Rodríguez, α-Al_2O_3 sapphire and rubies deformed by dual basal slip at intermediate temperatures (900–1300 °C) I. Dislocation organization, Acta Materialia 57 (2009) 2873.

[15] A. Nakamura, T. Yamamoto, Y. Ikuhara, Direct observation of basal dislocation in sapphire by HRTEM, Acta Materialia 50 (2002) 101.

[16] T. Geipel, K.P.D. Lagerlöf, P. Pirouz, A.H. Heuer, A zonal dislocation mechanism for rhombohedral twinning in sapphire (α-Al_2O_3), Acta Metallurgica et Materialia 42 (1994) 1367.

[17] M. Kronberg, Plastic deformation of single crystals of sapphire: basal slip and twinning, Acta Metallurgica 5 (1957) 507.

[18] J.D. Snow, A.H. Heuer, Slip systems in Al_2O_3, Journal of the American Ceramic Society 56 (1973) 153.

[19] E.R. Dobrovinskaya, L.A. Lytvynov, V. Pishchik, Properties of Sapphire, Sapphire, Springer, Boston, MA, US, 2009.

[20] A.H. Heuer, K.P.D. Lagerlof, J. Castaing, Slip and twinning dislocations in sapphire (α-Al_2O_3), Philosophical Magazine A 78 (1998) 747.

[21] E. Tochigi, N. Shibata, A. Nakamura, T. Yamamoto, Y. Ikuhara, Partial dislocation configurations in a low-angle boundary in α-Al_2O_3, Acta Materialia 56 (2008) 2015.

[22] G.I. Kanel, W.J. Nellis, A.S. Savinykh, S.V. Razorenov, A.M. Rajendran, Response of seven crystallographic orientations of sapphire crystals to shock stresses of 16–86 GPa, Journal of Applied Physics 106 (2009) 043524.

[23] C. Frick, B. Clark, S. Orso, A. Schneider, E. Arzt, Size effect on strength and strain hardening of small-scale [111] nickel compression pillars, Materials Science and Engineering A 489 (2008) 319.

[24] T.A. Parthasarathy, S.I. Rao, D.M. Dimiduk, M.D. Uchic, D.R. Trinkle, Contribution to size effect of yield strength from the stochastics of dislocation source lengths in finite samples, Scripta Materialia 56 (2007) 313.

[25] M.D. Uchic, D.M. Dimiduk, J.M. Florando, W.D. Nix, Sample dimensions influence strength and crystal plasticity, Science 305 (2004) 986.

[26] D.M. Dimiduk, M.D. Uchic, T.A. Parthasarathy, Size-affected single-slip behavior of pure nickel microcrystals, Acta Materialia 53 (2005) 4065.

[27] J.R. Greer, W.C. Oliver, W. Nix, Size dependence of mechanical properties of gold at the micron scale in the absence of strain gradients, Acta Materialia 53 (2005) 1821.

[28] J. Greer, W. Nix, Nanoscale gold pillars strengthened through dislocation starvation, Physical Review B (2006) 73.
[29] W. Nix, J. Greer, G. Feng, E. Lilleodden, Deformation at the nanometer and micrometer length scales: effects of strain gradients and dislocation starvation, Thin Solid Films 515 (2007) 3152.
[30] S. Korte, W.J. Clegg, Discussion of the dependence of the effect of size on the yield stress in hard materials studied by microcompression of MgO, Philosophical Magazine 91 (2011) 1150.
[31] F. Ostlund, P. Howie, R. Ghisleni, S. Korte, K. Leifer, W. Clegg, J. Michler, Ductile-brittle transition in micropillar compression of GaAs at room temperature, Philosophical Magazine 91 (2011) 1190.
[32] K. Wasmer, T. Wermelinger, A. Bidiville, R. Spolenak, J. Michler, In situ compression tests on micron-sized silicon pillars by Raman microscopy —stress measurements and deformation analysis, Journal of Materials Research 23 (2011) 3040.
[33] R. Ghisleni, J. Liu, R. Raghavan, P. Brodard, A. Lugstein, K. Wasmer, J. Michler, In situ micro-Raman compression: characterization of plasticity and fracture in GaAs, Philosophical Magazine 91 (2011) 1286.
[34] S.S. Brenner, Tensile strength of whiskers, Journal of Applied Physics 27 (1956) 1484.
[35] S.S. Brenner, Plastic deformation of copper and silver whiskers, Journal of Applied Physics 28 (1957) 1023.
[36] G. Richter, K. Hillerich, D.S. Gianola, R. Mönig, O. Kraft, C.A. Volkert, Ultrahigh strength single crystalline nanowhiskers grown by physical vapor deposition, Nano Letters 9 (2009) 3048.
[37] H. Bei, S. Shim, M.K. Miller, G.M. Pharr, E.P. George, Effects of focused ion beam milling on the nanomechanical behavior of a molybdenum-alloy single crystal, Applied Physics Letters 91 (2007) 111915.
[38] D. Kiener, C. Motz, M. Rester, M. Jenko, G. Dehm, FIB damage of Cu and possible consequences for miniaturized mechanical tests, Materials Science and Engineering A 459 (2007) 262.
[39] J. McCaffrey, M.W. Phaneuf, L.D. Madsen, Surface damage formation during ion-beam thinning of samples for transmission electron microscopy, Ultramicroscopy 87 (2001) 97.
[40] R. Maaβ, D. Grolimund, S. Van Petegem, M. Willimann, M. Jensen, H. Van Swygenhoven, T. Lehnert, M.A.M. Gijs, C.A. Volkert, E. T. Lilleodden, R. Schwaiger, Defect structure in micropillars using X-ray microdiffraction, Applied Physics Letters 89 (2006) 151905.
[41] H. Gao, C.S. Ozkan, W.D. Nix, J.A. Zimmerman, L.B. Freund, Atomistic models of dislocation formation at crystal surface ledges in $Si_{1-x}Ge_x$/Si (100) heteroepitaxial thin films, Philosophical Magazine A 79 (1999) 349.
[42] H. Bei, Y. Gao, S. Shim, E. George, G. Pharr, Strength differences arising from homogeneous versus heterogeneous dislocation nucleation, Physical Review B (2008) 77.
[43] G.E. Beltz, L.B. Freund, On the nucleation of dislocations at a crystal surface, Physica Status Solidi B 180 (1993) 303.
[44] F. Östlund, K. Rzepiejewska-Malyska, K. Leifer, L.M. Hale, Y. Tang, R. Ballarini, W.W. Gerberich, J. Michler, Brittle-to-ductile transition in uniaxial compression of silicon pillars at room temperature, Advanced Functional Materials 19 (2009) 2439.
[45] E. Schmid, W. Boas, Plasticity of Crystals with Special Reference to Metals, F.A. Hughes, London, 1950.
[46] E. Schmid, Beiträge zur physik und metallographie des magnesiums, Zeitschrift fuer Elektrochemie 37 (1931) 447.
[47] K.S. Ng, A.H.W. Ngan, Breakdown of Schmid's law in micropillars, Scripta Materialia 59 (2008) 796.
[48] J.M. Wheeler, R. Raghavan, J. Michler, In situ SEM indentation of a Zr-based bulk metallic glass at elevated temperatures, Materials Science and Engineering A 528 (2011) 8750.
[49] H. Zhang, B.E. Schuster, Q. Wei, K.T. Ramesh, The design of accurate micro-compression experiments, Scripta Materialia 54 (2006) 181.
[50] B. Perner, J. Kvapil, V. Stránský, J. Kvapil, Growth of sapphire by the kyropoulus method, Kristall und Technik 14 (1979) 661.
[51] S. Sarkar, T. Ballabh, T. Middya, A. Basu, T-matrix approach to effective nonlinear elastic constants of heterogeneous materials, Physical Review B 54 (1996) 3926.
[52] S. Shim, H. Bei, M.K. Miller, G.M. Pharr, E.P. George, Effects of focused ion beam milling on the compressive behavior of directionally solidified micropillars and the nanoindentation response of an electro-polished surface, Acta Materialia 57 (2009) 503.
[53] J.F. Ziegler, M.D. Ziegler, J.P. Biersack, SRIM – the stopping and range of ions in matter (2010), Nuclear Instruments and Methods in Physics Research Section B 268 (2010) 1818.
[54] C. McHargue, Ion beam modification of ceramics, Materials Science and Engineering A 253 (1998) 94.